Site-Selective Agonist Binding to the Nicotinic Acetylcholine Receptor from *Torpedo californica*†

Xing-Zhi Song, Iraida E. Andreeva, and Steen E. Pedersen*

Department of Molecular Physiology and Biophysics, Baylor College of Medicine, Houston, Texas 77030

Received December 20, 2002; Revised Manuscript Received February 8, 2003

ABSTRACT: Fluorescent energy transfer measurements of dansyl-C6-choline binding to the nicotinic acetylcholine receptor (AChR) from *Torpedo californica* were used to determine binding characteristics of the $\alpha\gamma$ and $\alpha\delta$ binding sites. Equilibrium binding measurements show that the $\alpha\gamma$ site has a lower fluorescence than the $\alpha\delta$ site; the emission difference is due to differences in the intrinsic fluorescence of the bound fluorophores rather than differences in energy transfer at the two sites. Stopped-flow fluorescence kinetics showed that dissociation of dansyl-C6-choline from the AChR in the desensitized conformation occurs 5−10-fold faster from the $\alpha\gamma$ site than from the $\alpha\delta$ site. The dissociation rates are robust for distinct protein preparations, in the presence of noncompetitive antagonists, and over a broad range of ionic strengths. Equilibrium fluorescent binding measurements show that dansyl-C6-choline binds with higher affinity to the $\alpha\delta$ site ($K = 3$ nM) than to the $\alpha\gamma$ site ($K = 9$ nM) when the AChR is desensitized. Similar affinity differences were observed for acetylcholine itself. The distinct dissociation rates permit the extent of desensitization to be measured at each site during the time course of binding. This sequential mixing method of measuring the desensitized state population at each agonist site can be applied to study the mechanism of AChR activation and subsequent desensitization in detail.

The nicotinic acetylcholine receptor (AChR)[1] from *Torpedo californica* is a pentameric ligand-gated ion channel that consists of four distinct, homologous subunits with $\alpha_2\beta\gamma\delta$ stoichiometry. Agonist binding occurs at two sites situated at interfaces between the α and γ subunits and between the α and δ subunits (*1*). The sites are similar with respect to the contributions of the α subunits and the conserved residues contributed by the γ and δ subunits. However, the γ and δ subunits also cause the sites to differ in the binding properties and their propensity to undergo conformational changes upon binding of agonists or competitive antagonists. There exist at least three conformations of the AChR: the resting state (R), the open state (O), and the desensitized state (D). After initial, low-affinity binding to the resting state has occurred, the agonist induces channel opening and subsequently desensitization of the AChR, with concomitant changes to higher binding affinity. For the resting conformation, ACh differs in the affinity of binding to the two sites by nearly 100-fold (*2*), whereas affinities of binding to the desensitized state appear to be similar (*3*).

The differences between the two sites are clearly observed by binding measurements of other agonists and competitive antagonists. The antagonist α-conotoxin MI binds with approximately 10^4-fold higher affinity for the $\alpha\delta$ site of the mouse AChR (*4*, *5*), whereas this difference is only 10-fold in favor of the $\alpha\gamma$ site in the *Torpedo* AChR (*5*). α-Conotoxin MI, however, does not influence the conformation of the AChR (*5*, *6*). D-Tubocurarine binds with 100−1000-fold higher affinity to the $\alpha\gamma$ site (*1*, *7*). It stabilizes the desensitized state to a lesser extent than full agonists (*8*, *9*) and can induce channel opening under some circumstances (*10*). Epibatidine is a full agonist that retains differential affinity for the two agonist sites of ∼50-fold in both the mouse (*11*) and, as shown below, the *Torpedo* AChR. By virtue of their affinity differences, these compounds are useful for determining the role of each site in the conformational transitions of the AChR.

Models for activation and desensitization of the AChR usually include concerted transitions between the resting, open, and desensitized states. Some models include an additional conformational state described as the intermediate state, I (*12*). This state has been included to account for a transient affinity of ACh between that of the equilibrium binding affinity and the concentration required to cause channel opening (*13*), and to account for the presence of fast and slow desensitization. This intermediate state represents a distinct, concerted transition of the AChR. An alternative model for explaining binding of the agonist to the mouse AChR (*6*, *14*) permits each of the two binding sites to exist in distinct states such that the $\alpha\gamma$ site would be desensitized and the $\alpha\delta$ site resting, or vice versa: $\alpha\gamma_D-\alpha\delta_R$ or $\alpha\gamma_R-\alpha\delta_D$. This scheme follows the allosteric description of Koshland et al. (*15*), which permits nonconcerted conformational transitions at each binding site. An advantage of this model is that it requires just a mixture of known conformations; no new conformations need to be invoked. Electrophysiological data are often adequately

† This research was supported in part by Robert A. Welch Foundation Grant Q-1406 and U.S. Public Health Service Grant NS35212. X.-Z.S. was supported in part by Training Grants HL07676 (institutional) and GM19672 (individual).

* To whom correspondence should be addressed. Telephone: (713) 798-3888. Fax: (713) 798-3475. E-mail: pedersen@bcm.tmc.edu.

[1] Abbreviations: ACh, acetylcholine; AChR, nicotinic acetylcholine receptor; α-BgTx, α-bungarotoxin; DC6C, dansyl-C6-choline.

10.1021/bi027405b CCC: $25.00
Published on Web 03/19/2003

modeled by concerted allosteric transitions that include sequential binding of agonists (*2*). Concerted schemes can also account for direct binding measurements of [^{3}H]ACh (*3*, *16*). However, recent electrophysiological characterization of desensitization provides evidence for as many as five distinct states (*17*). As attempts to correlate structure and function progress to atomic resolution, understanding the full spectrum of conformational states adopted by the AChR and whether these states represent unique concerted structures or the combinatorial effects of a more limited set of structures will be critical.

Distinct concerted conformational states should display unique affinities and kinetics of binding. Binding can be detected by the fluorescent ACh analogue dansyl-C6-choline (DC6C) and followed in greater detail, temporally, than with radioligand binding methods. DC6C displays complex binding kinetics with three to four distinct exponential components (*18*−*21*) for which a two-state kinetic mechanism with a concerted transition between the R and D states can largely account. The complex kinetics arise partly from binding to the desensitized state, from transient binding to the resting states, and from binding to the pore of the ion channel at the noncompetitive antagonist binding site (*21*). However, current models of DC6C binding have not tested directly whether the intermediate rates may arise from distinct, intermediate, concerted conformational states, from asymmetric, individual conformational changes in the binding sites, or from more mundane effects such as changes in quantum yield at individual sites or upon conformational changes.

Raines and Krishnan found that the population of the desensitized state can be monitored by its characteristically slow dissociation rate using a sequential mixing stopped-flow fluorescence protocol (*21*). We now extend these observations to measure the population of the desensitized conformation at each individual $\alpha\gamma$ and $\alpha\delta$ site based on distinct rates of dissociation. We also found that the fluorescence emission differs at the two sites, that dissociation occurs more rapidly from the $\alpha\gamma$ site, and that the desensitized sites differ in their affinities for DC6C and for ACh itself. These results present new information about the differences in agonist binding between the two sites and provide a method for examining the conformational transitions in greater detail.

EXPERIMENTAL PROCEDURES

Materials. AChR-enriched membranes were obtained from *T. californica* electric organ (Aquatic Research Consultants, San Pedro, CA) as described previously (*9*, *22*); specific binding activity was measured by [^{3}H]ACh binding and is reported as ACh binding sites per milligram of protein. DC6C was synthesized according to the method of Waksman et al. (*23*) as described previously (*24*). [^{3}H]ACh (90 Ci/mmol) was obtained from American Radiolabeled Chemicals (St. Louis, MO); [^{3}H]ACh (74 Ci/mol) was from Amersham Corp. (Piscataway, NJ). Proadifen (SKF-522) was obtained from Research Biochemicals (Natick, MA); carbamylcholine, (+)-epibatidine, diisopropyl fluorophosphonate, and phencyclidine were from Sigma-Aldrich (St. Louis, MO). D-Tubocurarine was from ICN (Aurora, OH). Other reagents were from standard sources.

Fluorescence Spectroscopy. DC6C binding to the AChR was monitored by changes in fluorescence intensity (λ_{em} = 557 nM) under conditions of energy transfer from protein aromatic residues (*23*). Fluorescence data were collected on an SLM 8000C fluorometer; the excitation light from a 350 W xenon short arc lamp was passed through an excitation monochromator and filtered with a UV-pass filter (Oriel 59152). Each sample was excited at 282 nm at a 2.0 nm bandwidth. To improve the signal, the emission light was collected directly through a 495 nm cut-on filter (Oriel 59492) without passing through a monochromator.

DC6C fluorescence assays were conducted either in the low-ionic strength buffer [20 mM Hepes (pH 7.0)] or in *Torpedo* physiological saline buffer, HTPS [250 mM NaCl, 5 mM KCl, 3 mM $CaCl_2$, 2 mM $MgCl_2$, and 20 mM Hepes (pH 7.0)]. Fluorescence inhibition isotherms were measured by titration of a mixture of DC6C and AChR-rich membranes with the competitive ligand. For measuring relative fluorescence, a 2 mL AChR-rich membrane solution with 50 nM ACh sites was incubated with DC6C for 1 h and then titrated with concentrated competitive ligand solutions. Excess carbamylcholine (1 mM) was used to define the nonspecific fluorescence of DC6C in parallel titrations. Measurements of $\alpha\gamma$ and $\alpha\delta$ site binding affinities were conducted using low concentrations of AChR-rich membranes (3 nM ACh binding sites) with varying concentrations of DC6C.

All the kinetic experiments were carried out with a stopped-flow instrument from KinTek Corp. (model SF-2001, Austin, TX). Fluorescence was excited at 290 or 282 nm with a 4 nm slit width using a 75 W xenon lamp. The emission signal was collected through a 495 nm cut-on filter. To measure dissociation kinetics, AChR-rich membranes (typically 100 nM ACh binding sites) were incubated with DC6C (typically 1 μM) for 1 h and loaded into one syringe, and excess carbamylcholine (typically 2 mM) was loaded into the other. Dissociation kinetics were measured by rapidly mixing the solutions in a volume ratio of 1:1. Individual mixing curves (3−12) were averaged to reduce noise. Sequential mixing experiments were carried out in the same instrument fitted with three syringes using a two-push protocol. The first push mixes the contents of two syringes and drives it into a fixed-volume delay line. The instrument pauses for a preprogrammed time and then delivers a second push that forces the content of the delay line to mix with the content of the third syringe and forces that mixture into the fluorescence flow cell.

Radioligand Binding. Inhibition of [^{3}H]ACh binding was carried out using a filtration assay. Samples typically contained AChR-rich membranes (2 nM ACh binding sites), 25 μM proadifen, varying concentrations of [^{3}H]ACh at 86 Ci/mmol or isotopically diluted to 8.6 Ci/mmol, and varying concentrations of D-tubocurarine in a total volume of 300 μL. Samples were dispensed using a Packard Instruments (Meriden, CT) MultiProbe II robot into 96-well, round-bottom, polypropylene microtiter plates (Fisher Scientific). After incubation at room temperature for 30 min, the samples were filtered through a Whatman GF/F filter sheet using a Packard Filtermate Cell harvester, 96 samples at a time. The filter had been pretreated with 1% polyethylenimine for 1 h and washed with phosphate-buffered saline. To avoid removal of bound ACh, the filters were not washed after filtration of the samples, but immediately placed in scintil-

lation vials for counting. Nonspecific binding was assessed in the presence of excess carbamylcholine (1 mM).

Data Analysis. The data from equilibrium DC6C fluorescence inhibition assays by D-tubocurarine and epibatidine were corrected for dilution by the titration volume and further corrected for inner filter effects using the following equation (*25*):

$$F_{corr} = F_{obs} \times 10^{(A_{ex}+A_{em})/2} \quad (1)$$

where F_{corr} and F_{obs} are the corrected and observed fluorescence intensities, respectively, and A_{ex} and A_{em} are the absorbance of D-tubocurarine at the excitation and emission wavelengths, respectively. The corresponding molar extinction coefficients for D-tubocurarine are as follows: $\epsilon_{282} = 7500\ M^{-1}\ cm^{-1}$ and $\epsilon_{500-600} < 0.5\ M^{-1}\ cm^{-1}$. The inner filter correction was significant only at the highest D-tubocurarine concentrations. In the case of epibatidine, no inner filter effects were observed.

The corrected fluorescence data were fit to models for inhibition at one or two sites:

$$F_{corr} = a/(1 + I/K_{app}) + F_{bcg}$$
$$F_{corr} = a_1/(1 + I/K_1) + a_2/(1 + I/K_2) + F_{bcg} \quad (2)$$

where I is the inhibitor concentration, K_1 and K_2 are the inhibition constants for sites 1 and 2, respectively, a_1 and a_2 are the amplitudes for sites 1 and 2, respectively, and F_{bcg} is the nonspecific fluorescence background, after correcting for inner filter effects as needed. a_1 and a_2 reflect the DC6C fluorescence at each site under the conditions of energy transfer. To determine the dissociation constants at each site for competing ligands, the inhibition constants were corrected using the Cheng and Prusoff (*26*) equation, $K_I = K_{app}K_D/(K_D + L)$, where K_D is the equilibrium dissociation constant for DC6C and L its concentration.

To determine affinities of DC6C and ACh for the desensitized conformation independently at each site, we analyzed the inhibition of binding by epibatidine and by D-tubocurarine. Two-site fits of the data give the amplitudes of binding, a_1 and a_2, to the $\alpha\gamma$ and $\alpha\delta$ sites, respectively. To analyze the differences in affinity for the two sites, the ratio of the amplitudes of binding, $a_{\alpha\gamma}$ and $a_{\alpha\delta}$, was fit to the following equation for various L values:

$$a_{\alpha\gamma}/a_{\alpha\delta} = A(K_{D\alpha\delta} + L)/(K_{D\alpha\gamma} + L) \quad (3)$$

where L represents the DC6C or ACh concentration and A the ratio of amplitudes at saturating ligand concentrations. This equation can be justified by assuming independent binding at each site and taking the ratio of the individual binding equations $a_{\alpha\gamma} = R_0L/(K_{D\alpha\gamma} + L)$ and $a_{\alpha\delta} = R_0L/(K_{D\alpha\delta} + L)$, where R_0 is the AChR concentration.

DC6C isotherm titration data were fit to the Hill equation $\{F_{corr} = a/[1 + (K/L)^n]\}$. L is the DC6C concentration and n the Hill coefficient. For curves without cooperativity, n was fixed to 1, which reduces the expression to the single-site binding equation. Binding isotherm data were also fit to an equation describing binding as a function of the total ligand concentration added, L_0, and the receptor concentration, R_0. This formula accounts for the loss of free ligand due to binding a single site when ligand is not in excess over the receptor concentration (*24*):

$$F_L = \frac{C}{2}[K + R_0 + L_0 - \sqrt{(K + R_0 + L_0)^2 - 4R_0L_0}] \quad (4)$$

Dissociation rate data were fit to the double-exponential equation

$$F = A_1e^{-k_{1-}t} + A_2e^{-k_{2-}t} + C \quad (5)$$

where F is the observed fluorescence intensity, k_{1-} and k_{2-} are the rate constants for the fast and slow dissociation components, respectively (s^{-1}), A_1 and A_2 are their respective fluorescence amplitudes, respectively, and C represents the final level of observed fluorescence intensity. Fitting to single exponentials was to the same equation with an A_2 of 0.

Data Modeling. To determine whether the individual DC6C K_D values measured by the binding amplitude ratio method, as described above, or calculated from the ratio of kinetic constants, agreed with our binding isotherm data, we compared the theoretical binding based on those constants to our binding isotherm data. Because the data were collected under conditions where the total DC6C concentration, L_0, differed significantly from the actual free DC6C concentration, it was necessary to determine the expected binding in terms of the total ligand concentration and the receptor concentration R_0. However, eq 4, which is the appropriate solution for a single binding site, does not apply for two binding sites. Therefore, we solved this problem for two independent sites by calculating a value for the free ligand concentration, L, in terms of L_0, R_0, $K_{D\alpha\delta}$, and $K_{D\alpha\gamma}$, as the real root of a cubic equation. From this solution, we could back-calculate the expected populations of the bound states to model the binding.

RESULTS

DC6C Fluorescence Differs at the Two AChR Binding Sites. To fully characterize the kinetics of binding of DC6C at the two individual sites, it is important to determine the relative signals arising at each site. Therefore, we first examined whether the fluorescence emission intensity differs for the $\alpha\gamma$ and $\alpha\delta$ sites by titration of DC6C-bound AChR with increasing concentrations of the site-selective ligands D-tubocurarine and epibatidine. Both ligands bind the $\alpha\gamma$ site with higher affinity than the $\alpha\delta$ site. The fluorescence titration data show inhibition of DC6C binding with increasing concentrations of competing D-tubocurarine or epibatidine (Figure 1A). In parallel experiments carried out in the presence of carbamylcholine, the fluorescence decreases at the higher D-tubocurarine concentrations due to inner filter effects; this was not seen with epibatidine because it does not absorb significantly at the 282 nm excitation wavelength. After correction for the inner filter effect, for volume dilution during titration, and for subtraction of background fluorescence as defined by the presence of carbamylcholine, the data were fit to an equation for inhibition at two independent sites (eq 2) with variable site stoichiometries, a_1 and a_2 (Figure 1B). These values describe the relative light emission from each site. To ensure that these values reflected the relative DC6C fluorescence at each site, it was important to determine that the two sites were equally saturated by DC6C.

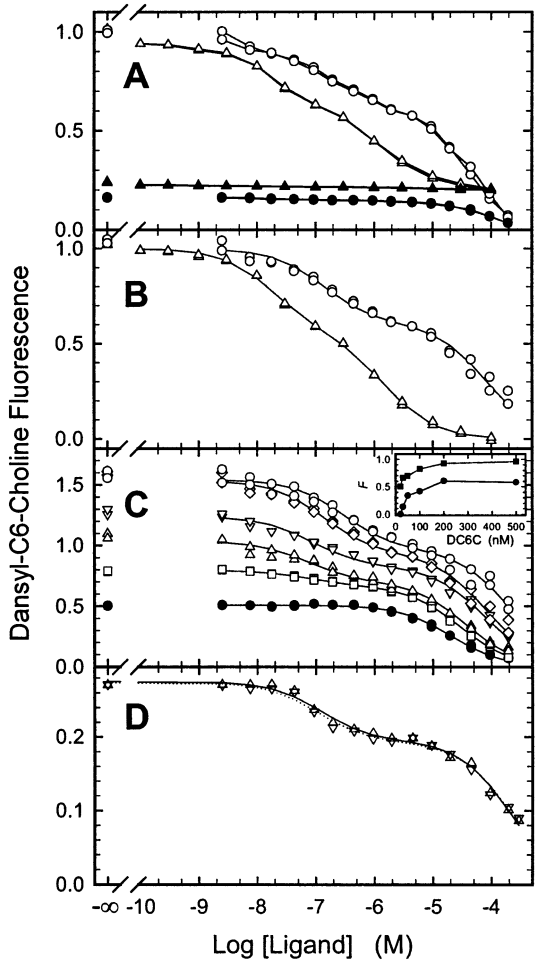

FIGURE 1: DC6C fluorescence differs at the $\alpha\gamma$ and $\alpha\delta$ sites. (A) AChR-rich membranes (50 nM ACh sites in 2 mL of HTPS) were incubated with 200 nM DC6C, for D-tubocurarine, or with a 500 nM DC6C/10 μM proadifen mixture, for epibatidine. Duplicate fluorescence inhibition curves were measured by titration with increasing concentrations of D-tubocurarine (○ and ●) or epibatidine (△ and ▲) in the absence (○ and △) or presence (● and ▲) of 1 mM carbamylcholine, as described in Experimental Procedures, with a λ_{ex} of 282 nm. Data were normalized to the first, untitrated point. (B) After correction for dilution and inner filter effects and subtraction of background fluorescence, the titration data from panel A were fit to a model for inhibition at two binding sites (—). For D-tubocurarine (○), $K_1 = 140$ nM and $K_2 = 83$ μM. For epibatidine (△), $K_1 = 19$ nM and $K_2 = 1.5$ μM. Using the K value for DC6C binding (see Table 3) and the Cheng and Prusoff correction for DC6C occupancy, the binding constants for epibatidine binding to desensitized $\alpha\gamma$ and $\alpha\delta$ sites are 0.34 ($K_{I\alpha\gamma}$) and 8.9 nM ($K_{I\alpha\delta}$), respectively. (C) AChR-rich membranes (50 nM ACh sites) were titrated with D-tubocurarine in 20 (●), 30 (□), 50 (△), 100 (▽), 200 (◇), or 500 nM (○) DC6C in HTPS. The data shown were corrected for dilution and inner filter effects, and background fluorescence was subtracted. Each curve was fit to the two-site inhibition model (—). In the inset, the fluorescence corresponding to binding to the $\alpha\gamma$ site (a_1, ●) and the $\alpha\delta$ site (a_2, ■) from each curve was plotted against the DC6C concentration. (D) AChR-rich membranes (50 nM ACh binding sites) were incubated in 100 nM DC6C and 10 μM proadifen and titrated with D-tubocurarine; fluorescence data were collected with a λ_{ex} of 335 nm. The data show two duplicate titrations after correction for dilution and subtraction of background fluorescence. The solid and dotted curves show the best fits to models for inhibition at two binding sites for each titration. $K_1 = 96 \pm 23$ nM, and $K_2 = 222 \pm 12$ μM (averages of four experiments).

Therefore, D-tubocurarine titrations were carried out at various concentrations of DC6C, and the corrected data were fit to determine a_1 and a_2 (Figure 1C). A replot of the a_1 and a_2 values versus the DC6C concentration shows that they reach asymptotic limits at high concentrations (Figure 1C, inset). Comparison of a_1 and a_2 shows that DC6C bound to the $\alpha\delta$ site emits ~50% more light than when bound to the $\alpha\gamma$ site (Table 1).

Table 1: Relative Fluorescence of DC6C at the $\alpha\gamma$ and $\alpha\delta$ Sites

	$Q_{rel} \times 100$[a]	
method	$\alpha\gamma$	$\alpha\delta$
dTC[b]	39 ± 2.6[c]	61 ± 2.6
epibatidine	40 ± 6	60 ± 5.7
dTC, $\lambda_{ex} = 335$ nm	29 ± 1.7	71 ± 1.7

[a] The relative fluorescence is given as the percent of total fluorescence from both sites. [b] Relative fluorescence yields were measured by inhibition of fluorescence with D-tubocurarine (dTC) or epibatidine under energy transfer conditions, or by inhibition with dTC using direct excitation of DC6C at 335 nM, as shown in Figure 1. [c] Errors are the standard deviations of four independent determinations.

Martinez et al. (*27*) determined fluorescent lifetimes for bound DC6C and observed longer lifetimes at the $\alpha\gamma$ site, suggesting that this site should have a higher quantum yield, rather than the $\alpha\delta$ site. However, they used an excitation wavelength of 330 nm, which excites the dansyl fluorophore directly, whereas we carried out excitation of DC6C by energy transfer from aromatic residues using 282 nm light. Therefore, we carried out a D-tubocurarine titration experiment using an excitation wavelength of 335 nm. This condition gives a substantially smaller signal-to-background ratio, but does yield specific fluorescence changes (Figure 1D). Determination of a_1 and a_2 shows an even higher relative fluorescence for the $\alpha\delta$ site than seen by energy transfer (Table 1). Differences in excitation wavelength, therefore, do not account for the difference between our results and those of Martinez et al. (*27*). This experiment also shows that the difference in DC6C fluorescence emission at the two sites is not due to differences in energy transfer. The distinct fluorescent yields, therefore, likely reflect differences in the microenvironment, in the local quenching of the fluorophore, or in DC6C absorbance.

The data in Figure 1C show that there was little or no apparent binding to the $\alpha\gamma$ site seen by D-tubocurarine inhibition at concentrations of DC6C lower than the concentration of binding sites (●). This observation could reflect either a substantially higher intrinsic affinity for the $\alpha\delta$ site or displacement of DC6C from the $\alpha\gamma$ site by D-tubocurarine with displaced DC6C rebinding to free $\alpha\delta$ sites. In the latter case, rebinding to the $\alpha\delta$ site would occur because D-tubocurarine binding to the $\alpha\gamma$ site will desensitize the AChR (*9*) and consequently increase the affinity of the $\alpha\delta$ site for DC6C. To distinguish between these two explanations, we determined DC6C binding isotherms in the presence and absence of 1 μM D-tubocurarine (Figure 2A). This concentration is sufficient to bind greater than 95% of the $\alpha\gamma$ sites, but less than 20% of the $\alpha\delta$ sites.

In the absence of D-tubocurarine, DC6C binds cooperatively to the two sites [Figure 2A (○)], as expected (*24*), with a Hill coefficient of 1.3−1.6. In the presence of D-tubocurarine, binding can be fit to a single-site, noncooperative mechanism with a lower K value. This leads to the peculiar observation that the presence of the competitive inhibitor causes more DC6C binding at low DC6C concen-

Table 2: Dissociation Kinetics of DC6C Induced by Various Competing Agonists[a]

		amplitude[b]		rate (s^{-1})	
ligand	NCA	A_1	A_2	k_{1-}	k_{2-}
TMA	none	39 ± 2[c]	61 ± 2	2.3 ± 0.19	0.269 ± 0.009
	tetracaine	39 ± 2	61 ± 1	2.6 ± 0.09	0.277 ± 0.005
	proadifen	39 ± 2	61 ± 0.4	4.3 ± 0.17	0.284 ± 0.002
	phencyclidine	40 ± 2	60 ± 2	3.6 ± 0.3	0.35 ± 0.01
ACh	none	37 ± 2.5	63 ± 2	1.09 ± 0.12	0.21 ± 0.01
	tetracaine	37 ± 2	63 ± 2	1.1 ± 0.1	0.21 ± 0.01
	meproadifen	36 ± 0.4	64 ± 1	2.0 ± 0.1	0.21 ± 0.005
	phencyclidine	38 ± 1	62 ± 2	1.65 ± 0.01	0.276 ± 0.002
carbamylcholine	none	37 ± 4	63 ± 4	0.93 ± 0.19	0.188 ± 0.008
	tetracaine	32 ± 2	68 ± 4	1.2 ± 0.2	0.19 ± 0.01
	proadifen	36 ± 1	64 ± 3	1.5 ± 0.2	0.19 ± 0.01
	phencyclidine	38 ± 4	62 ± 6	1.4 ± 0.4	0.24 ± 0.02

[a] AChR-rich membranes (100 nM) were preincubated in HTPS with 1 μM DC6C and with the indicated noncompetitive antagonist (NCA) at 30 μM. Fluorescent decays were measured upon stopped-flow rapid mixing with an equal volume of a solution containing the same concentration of NCA and the indicated ligand, 100 mM tetramethylammonium (TMA), 2 mM carbamylcholine, or 2 mM ACh. [b] Amplitudes are given as a percent of the total fluorescent decay signal. [c] Errors are the standard deviations of three determinations.

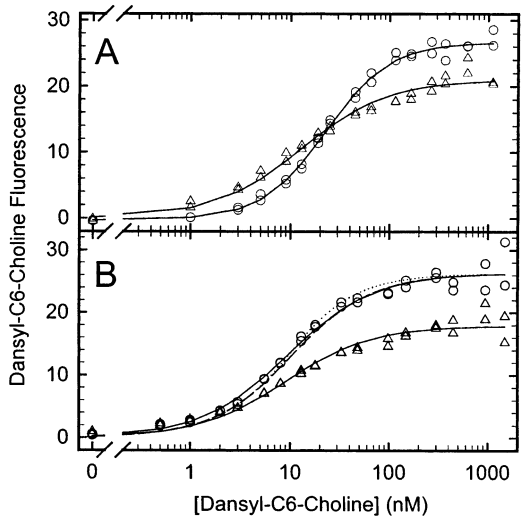

FIGURE 2: D-Tubocurarine desensitizes the $\alpha\delta$ site by binding the $\alpha\gamma$ site. AChR-rich membranes (10 nM ACh binding sites) were incubated in HTPS in the presence (△) or absence (○) of 1 μM D-tubocurarine and in the absence (A) or presence (B) of 10 μM proadifen and then titrated with the indicated concentrations of DC6C. The duplicate titrations were corrected for dilution and for background fluorescence, as determined from parallel titrations, including 1 mM carbamylcholine. The data were fit to single-site binding equations, except for the curve in the absence of D-tubocurarine and proadifen, which was fit to the Hill equation (—). (A) With no D-tubocurarine, $K = 23$ nM and $n = 1.35$; with 1 μM D-tubocurarine, $K = 13$ nM. (B) With no D-tubocurarine, $K = 9.4$ nM; with 1 μM D-tubocurarine, $K = 8.9$ nM. The data in the absence of D-tubocurarine and presence of proadifen in panel B were also fit to eq 4 to yield a K of 4.3 nM (curve not shown). The expected level of binding was calculated from a two-site model (see Data Modeling in Experimental Procedures) and the K values for each site as determined by the amplitude ratio method (•••) or calculated from the ratio of kinetic constants (− − −; see Table 3 below).

trations of 1−20 nM, not less. A similar experiment carried out in the presence of proadifen, a desensitizing noncompetitive antagonist, shows apparent single-site binding in the presence or absence of D-tubocurarine, with similar affinities (Figure 2B, $K \sim 9$ nM). In this case, D-tubocurarine diminishes the level of DC6C binding at all concentrations. In the presence of D-tubocurarine, DC6C binds predominantly the $\alpha\delta$ site; the affinities for this site are similar in the presence and absence of proadifen (compare triangles in panels A and B of Figure 2). These observations favor the model of D-tubocurarine binding to the $\alpha\gamma$ site and causing desensitization of the AChR, resulting in increased affinity and enhanced binding at the $\alpha\delta$ site. The data for DC6C binding in the presence of proadifen, without D-tubocurarine, show a single class of binding sites, which suggests similar affinities for DC6C at the two sites when they are desensitized. However, as we shall show below, a small difference between the desensitized affinities at the $\alpha\gamma$ and $\alpha\delta$ sites that could not be detected by these experiments does exist.

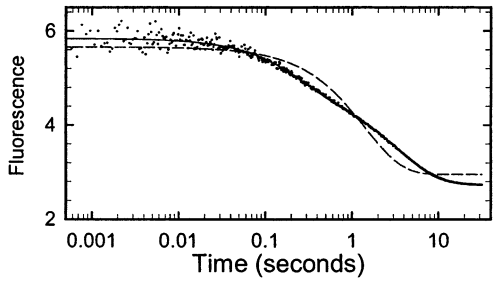

FIGURE 3: Dissociation kinetics of DC6C are biphasic. AChR-rich membranes (100 nM ACh binding sites) were preincubated with 1 μM DC6C in 20 mM Hepes, 250 mM NaCl, and 10 μM proadifen for 1 h and rapidly mixed with 2 mM carbamylcholine in the same solution. The data (•) were fitted to equations for single-exponential decay (− − −) and double-exponential decay (—, eq 4). The rate for single-exponential decay (k_{-}) was 1.25 s^{-1}. The rates for the double-exponential decay were 4.1 (k_{1-}) and 0.28 s^{-1} (k_{2-}).

DC6C Dissociates Faster from the $\alpha\gamma$ Site. The kinetics of dissociation of DC6C from the AChR were examined by rapid-mixing stopped-flow fluorescence. Two solutions were mixed. The first contained AChR-rich membranes preequilibrated with DC6C; the second contained a high concentration of competitive inhibitor, typically 2 mM carbamylcholine. Once mixing had taken place, the dissociation of DC6C was observed to undergo biphasic decay (Figure 3) that could be well fit by a two-exponential decay function (eq 4). The data were poorly fit by a single exponential. The two-exponential fit yielded distinct rate constants near 4.1 and 0.28 s^{-1} (Table 2). These rates had distinct amplitudes, the faster rate having the smaller amplitude. The biphasic nature could be due to a number of causes, including receptor heterogeneity, conformational

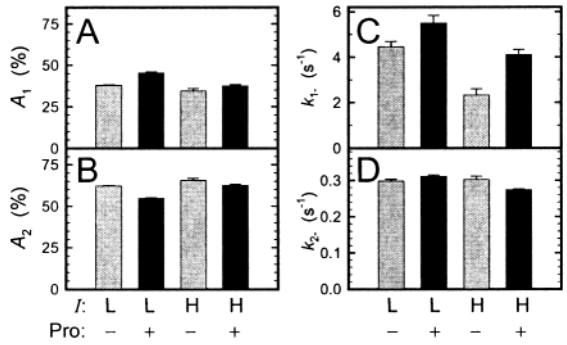

FIGURE 4: Effects of ionic strength and proadifen on DC6C dissociation kinetics. AChR-rich membranes (100 nM ACh binding sites) were pre-equilibrated with 1 μM DC6C and then rapidly mixed with 2 mM carbamylcholine in the stopped flow. Dissociation kinetics were measured by changes in fluorescence intensity and the data fit to two-exponential decays. The normalized amplitudes of the fast (A) and slow (B) components and the corresponding rate constants (C and D) were averaged over five different AChR-rich membrane preparations; error bars indicate the standard deviations. Dissociation curves were determined in the absence (gray bars, indicated by −) and presence of 10 μM proadifen (black bars, indicated by +), in low-ionic strength buffer [L; 20 mM Hepes (pH 7.0)] and in high-ionic strength buffer [H; 250 mM NaCl and 20 mM Hepes (pH 7.0)].

changes during dissociation, the presence of distinct conformational states, or distinct off-rates at the two sites. Therefore, we further examined the amplitudes and rates of DC6C dissociation under several different conditions.

We examined five different *Torpedo* AChR-rich membrane preparations and compared the effects of ionic strength and the presence of proadifen on dissociation rates and amplitudes (Figure 4). Proadifen and low ionic strength are known to promote a high-affinity conformation of the AChR (*8*, *24*). The standard deviation among membrane preparations was small (see the error bars in Figure 4) for both amplitudes and rates. The relative amplitudes of the fast (Figure 4A) and slow (Figure 4B) phases varied no more than 10% among the four experimental conditions. The slower rate of dissociation (k_{2-}, Figure 4D) also varied less than 10%. The biggest variation was observed for k_{1-}; at high ionic strength, without proadifen the values were substantially slower (Figure 4C). This condition favors the resting state of the AChR, which has lower net affinity and a potentially faster dissociation rate. However, we observe slower dissociation rates rather than faster, suggesting instead that conditions that favor desensitization enhance this dissociation rate.

The dissociation rates appeared to be robust and therefore were likely characteristic of a stable state at equilibrium. Binding of agonists, such as DC6C, promotes the desensitization of the receptor (*16*, *28*), suggesting that the observed dissociation phases were from this state. To further test this interpretation, we examined dissociation rates in the presence of noncompetitive antagonists that bind in the channel pore. These compounds have been shown to affect the affinity of agonists allosterically. Proadifen, meproadifen, and phencyclidine increase agonist affinity, whereas tetracaine decreases agonist affinity (*3*). These effects have been interpreted as preferential stabilization of the desensitized or resting states, respectively, but could also result from stabilization of distinct conformational states. We expect that rates of dissociation from the desensitized state should not be dramatically dependent on the presence of noncompetitive antagonists unless they affect the rate of conformational interchange or stabilize unique conformational states. In addition, dissociation from the desensitized state should be independent of the nature of the competing ligand.

Table 2 shows the relative amplitudes and rates for three agonists used as a competing ligand: tetramethylammonium, ACh, and carbamylcholine. For each agonist, data were also collected in the presence of three noncompetitive antagonists. The rates were similar for all three agonists, although they were somewhat faster when tetramethylammonium was used as the competing ligand: approximately 2-fold faster for k_{1-} and 1.5-fold faster for k_{2-}. This effect might be due to the 17% increase in ionic strength caused by the addition of tetramethylammonium, but from Figure 4, increasing ionic strength had virtually no effect on k_{2-} and decreased k_{1-} slightly rather than increasing it. The dissociation rates were found to depend weakly on the concentration of the competing agonist carbamylcholine (data not shown). The faster rate, k_{1-}, was more sensitive than k_{2-}, and this rate increased only at carbamylcholine concentrations of >10 mM. Below that concentration, rates were stable until concentrations became too low to effectively displace all the DC6C. Phencyclidine and proadifen both increased k_{1-} to a small extent (2-fold), but only phencyclidine changed k_{2-} (~25%). Although different agonists, noncompetitive antagonists, and conditions can influence the dissociation rates, the changes were all modest, whereas the fast and slow rates consistently differed from each other by 5−10-fold. The data suggest that the dissociation rates are characteristic for the desensitized state.

The data in Table 2 and panels A and B of Figure 4 show that the relative amplitudes corresponding to each rate are consistent over the conditions that were tested. We also noted that the relative amplitudes correlated with the differences in fluorescence at the two binding sites (Table 1). This suggested that the rate with a lower amplitude, k_{1-}, reflects dissociation from the $\alpha\gamma$ site and that k_{2-} reflects dissociation from the $\alpha\delta$ site. This correlation was tested by carrying out dissociation rate experiments where the AChR-rich membrane mixture contained varying concentrations of the site-selective inhibitors α-conotoxin MI, D-tubocurarine, or epibatidine. Each ligand binds with higher affinity to the $\alpha\gamma$ site but varies in its propensity to desensitize the AChR. α-Conotoxin MI has no apparent effect on the conformational state (*5*); D-tubocurarine partly desensitizes the AChR (*9*), and the agonist epibatidine desensitizes it fully (*11*). Figure 5A shows the inhibition of amplitudes A_1 and A_2 from the dissociation rate analysis as a function of inhibitor concentration. The smaller, faster amplitude A_1 is inhibited at lower concentrations of either epibatidine or D-tubocurarine, whereas the larger, slower amplitude A_2 is inhibited only at substantially higher ligand concentrations. Similar results were obtained for α-conotoxin MI (Figure 5B). For each ligand, the difference in EC_{50} between the two amplitudes corresponded to the expected differences in affinity for the two sites: 300−600-fold for D-tubocurarine, 20−50-fold for epibatidine (Figure 1B), and 10-fold for α-conotoxin MI. The dissociation rates were not systematically affected by the presence of the competitive inhibitors (data not shown). The results show that fast dissociation, k_{1-}, is from the $\alpha\gamma$ site and slow dissociation, k_{2-}, is from the $\alpha\delta$ site.

The $\alpha\delta$ Site Has a Higher DC6C Affinity Than the $\alpha\gamma$ Site, in the Desensitized State. The data displayed in Figure

Table 3: DC6C Association, Dissociation, and Equilibrium Constants for Desensitized $\alpha\gamma$ and $\alpha\delta$ Sites

	in HTPS	in 20 mM Hepes	in 20 mM Hepes and 250 mM NaCl
k_+ (s^{-1} M^{-1})[a]	$(6.8 \pm 0.24) \times 10^7$	$(1.8 \pm 0.5) \times 10^8$	$(9.8 \pm 2.9) \times 10^7$
k_-, $\alpha\gamma$ (s^{-1})[b]	1.2 ± 0.25	4.6 ± 0.6	4.5 ± 1.3
k_-, $\alpha\delta$ (s^{-1})[b]	0.20 ± 0.01	0.30 ± 0.01	0.31 ± 0.01
k_-/k_+, $\alpha\gamma$ (nM)[c]	18 ± 4[f]	26 ± 9	46 ± 21
K_D, $\alpha\gamma$ (nM)[d]	9.4 ± 1.7[g]		
k_-/k_+, $\alpha\delta$ (nM)[c]	2.9 ± 4[f]	1.7 ± 1.3	3.2 ± 2.5
K_D, $\alpha\delta$ (nM)[d]	3.2 ± 0.7[g]		
K_D, +pro (nM)[e]	11 ± 2	1.29 ± 0.60	4.46 ± 0.59
K, isotherm (nM)[e]	31 ± 7	0.83 ± 0.38	28.4 ± 1.8

[a] Determined from the data shown in Figure 6 and from similar experiments carried out in the other buffers. [b] k_- values for $\alpha\gamma$ and $\alpha\delta$ sites were determined essentially as described in the legends of Figures 3 and 4. [c] Calculated from the data in the higher rows. [d] K_D values for individual sites in the desensitized state were determined from the data shown in Figure 7. [e] Equilibrium dissociation constants in the absence (K) or presence of proadifen (K_D) were determined by DC6C titration of 5 or 10 nM suspensions of AChR-rich membranes, essentially as described in Figure 2 and the Experimental Procedures. K_D values were from the best fits to the Hill equation with an n of 1. [f] Standard deviations for calculated values were determined by propagation of errors. [g] Standard deviations determined from nonlinear regression as shown in Figure 7.

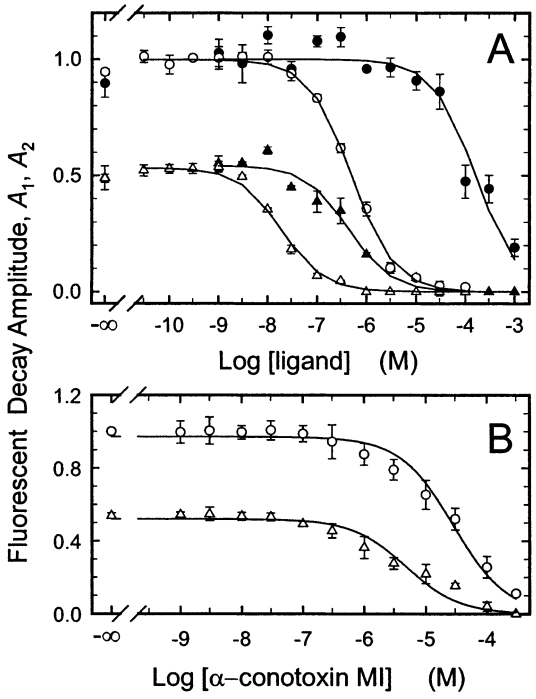

FIGURE 5: Fast and slow dissociation occurs from the $\alpha\gamma$ and $\alpha\delta$ sites, respectively. (A) AChR-rich membranes (100 nM) in HTPS were preincubated with 400 nM DC6C, 10 μM proadifen, and varying concentrations of epibatidine (○ and △) or D-tubocurarine (● and ▲). (B) AChR-rich membranes (50 nM) in HTPS were preincubated with 120 nM DC6C, 10 μM proadifen, and varying concentrations of α-conotoxin MI (○ and △). DC6C dissociation kinetics were measured by stopped-flow rapid mixing with 2 mM carbamylcholine as shown in Figure 3. Dissociation data were fitted to a two-exponential equation to determine the amplitudes of fast (A_1; △ and ▲) and slow (A_2; ○ and ●) decay. The amplitudes are plotted as the averages and standard deviations of four independent determinations, normalized to the higher, A_2 amplitude control (no competing ligand) value. The concentration dependence was fitted to eq 2 for single-site inhibition. The corresponding K values are as follows: $K_1 = 0.43$ μM and $K_2 = 160$ μM for D-tubocurarine, $K_1 = 19$ nM and $K_2 = 500$ nM for epibatidine, and $K_1 = 4.7$ μM and $K_2 = 28$ μM for α-conotoxin MI.

5 show that fast dissociation of DC6C is from the desensitized $\alpha\gamma$ site and slow dissociation is from the desensitized $\alpha\delta$ site. The 5−10-fold difference in dissociation rates suggests that the affinities of the desensitized states should differ correspondingly, unless the association rates compensate. However, the binding isotherm determined in the presence of proadifen, included to promote desensitization, was consistent with single-site binding with a K_D of 9−11 nM as determined by fitting to the Hill equation (Figure 2B and Table 3). To determine whether the measured association and dissociation rates agreed with the equilibrium DC6C binding measurement, we first measured the rate constant for association with AChR-rich membranes. Measurements were taken in the presence of proadifen to induce desensitization. Association kinetics were measured in the stopped flow at various DC6C concentrations, and each curve was fit to a sum of three exponentials (Figure 6A). The fastest component was the largest and presumably corresponded to fast binding to the desensitized state of the AChR (*29*). The other components presumably corresponded to induced desensitization of the residual, resting state AChR. The rates determined at various DC6C concentrations were plotted against DC6C concentration to determine the second-order rate constant for binding (Figure 6B). This value was 6.8×10^7 M^{-1} s^{-1} (Table 3), which is near the diffusion-limited rate for association ($\sim 10^8$ M^{-1} s^{-1}).

There was no evidence that there were distinct association rates for the $\alpha\gamma$ and $\alpha\delta$ sites because the rapid phase of association was described well by one exponential component (Figure 6A). Nonetheless, it was possible that a discrete component could be missed because the rates were similar to each other or the results biased by the distinct fluorescent yields of the sites. Therefore, we examined the rate of binding at each site, individually, utilizing the distinct dissociation rates to measure the amount of ligand bound to desensitized sites. The following sequential mixing stopped-flow protocol was used. AChR-rich membranes preincubated with proadifen were rapidly mixed with DC6C, and the mixture was forced into a delay line. Flow was halted for a preset period to allow binding to occur in the delay line. The mixture in the delay line was then mixed with a high concentration of carbamylcholine from the third syringe, to induce DC6C dissociation, and forced into the flow cell to measure fluorescence decay. The fast and slow amplitudes of dissociation yield the amount of fluorescence due to binding to desensitized $\alpha\gamma$ and $\alpha\delta$ sites, respectively. Measurements of these amplitudes with varying delay times show that binding to each site occurs at similar rates (Figure 6C). The rates correspond to bimolecular rate constants of 8.5×10^7 M^{-1} s^{-1} for the $\alpha\gamma$ site and 7.5×10^7 M^{-1} s^{-1} for the $\alpha\delta$ site; they are consistent with the bimolecular association rate constant determined in Figure 6B.

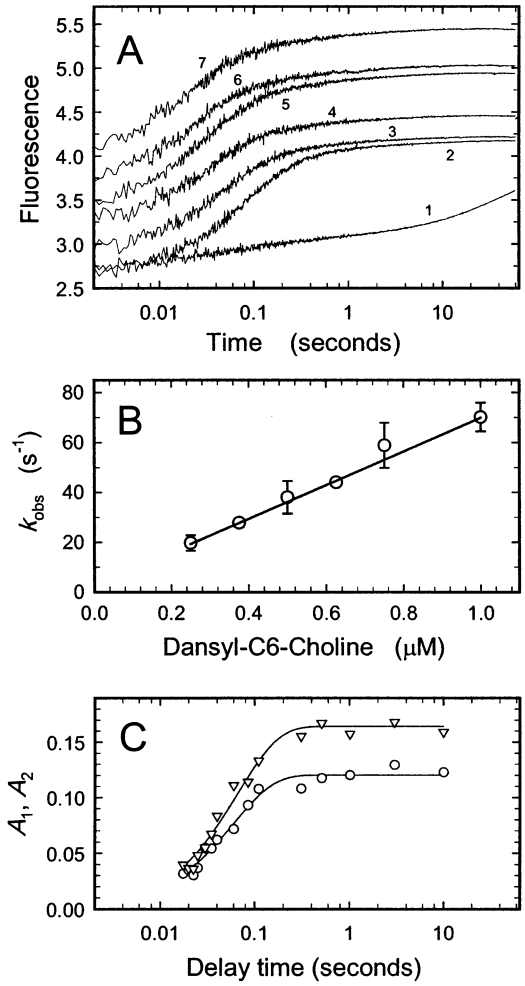

FIGURE 6: Association kinetics of DC6C binding. (A) AChR-rich membranes (200 nM) in HTPS were rapidly mixed in the stopped flow with an equal volume of 0.5 (1 and 2), 0.75 (3), 1 (4), 1.25 (5), 1.5 (6), or 2.0 μM DC6C (7). Reactions were carried out in the absence (trace 1) or presence of 25 μM proadifen (traces 2−7). Fluorescence changes were recorded for 30 s following mixing. Each curve was fit to a sum of three exponentials (not shown). (B) The fastest exponential rate constant from each curve was plotted against the corresponding final DC6C concentration. Each point is the average of three independent experiments at the same concentration; errors are standard deviations. The best fit to a straight line yielded a slope of 6.8×10^7 M^{-1} s^{-1} with an intercept of 2.4 s^{-1}. (C) AChR-rich membranes (100 nM sites) were preincubated with 50 μM proadifen. They were mixed in the stopped flow with an equal volume of 400 nM DC6C and 50 μM proadifen and held in the delay line for the indicated period. This mixture was then mixed with $^1/_2$ volume of 3 mM carbamylcholine and 50 μM proadifen to induce dissociation. Individual dissociation curves were fit to two-exponential decays (eq 4) to determine the rate and amplitude for each component. The amplitudes, A_1 and A_2, are plotted vs delay time; each set of data was fitted to a single-exponential increase (—) to yield the following rates: $k_1 = 17.1$ and $k_2 = 15.0$.

Determination of the dissociation and association rates for binding allows us to calculate the equilibrium dissociation constant for binding to the desensitized state from the relationship $K_D = k_-/k_+$. The K_D values calculated in this way, 18 and 2.9 nM for the $\alpha\gamma$ and $\alpha\delta$ sites, respectively, differ significantly from the single-site value measured by binding isotherm (11 nM, Table 3). The discrepancy is more pronounced for the $\alpha\gamma$ site under the buffer conditions of low and high ionic strength. However, discriminating binding site differences of less than 10-fold by analysis of binding isotherms requires a precision that is difficult to obtain with our methods. Therefore, it was possible that differences in binding between the two sites were masked within the binding isotherm.

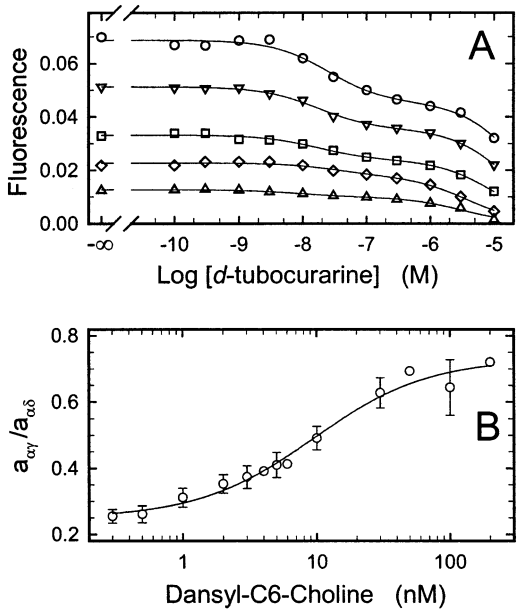

FIGURE 7: DC6C binds with higher affinity to the $\alpha\delta$ site than the $\alpha\gamma$ site of the desensitized AChR. (A) AChR-rich membranes (3 nM) were incubated in HTPS, 30 μM proadifen, and the indicated concentrations of D-tubocurarine with the following concentrations of DC6C: 0.5 (△), 1 (◇), 2 (□), 4 (▽), and 5 nM (○). Steady state DC6C fluorescence was measured for each sample and for parallel samples containing 1 mM carbamylcholine, which were subtracted. The data were fitted to the two-site inhibition equation (eq 2, —), with an F_{bcg} of 0, to determine the fluorescence contribution from each site, $a_{\alpha\gamma}$ and $a_{\alpha\delta}$. (B) Fluorescence ratios, $a_{\alpha\gamma}/a_{\alpha\delta}$, were combined from six experiments with DC6C concentrations varying up to 200 nM. The plot shows the averages, standard deviations, and the best fit to eq 3 (points without error bars are single determinations). The K values from the fit are as follows: $K_{D\alpha\delta} = 3.2 \pm 0.7$ nM and $K_{D\alpha\gamma} = 9.4 \pm 1.7$ nM. The asymptotic value at high DC6C concentrations, $A = 0.73$, should equal the ratio of fluorescent yields, $Q_{\alpha\gamma}/Q_{\alpha\delta} = 0.66$ (Table 1).

To test this possibility, we examined DC6C binding to desensitized $\alpha\gamma$ and $\alpha\delta$ sites at low ligand concentrations (Figure 7). Under these conditions, DC6C will bind each site to an extent nearly proportional to its affinity, and we can detect differences in affinity by measuring the amount bound at each site. To determine the amount of binding at each site, we carried out inhibition titrations with increasing concentrations of D-tubocurarine and measured the amount of binding at each site by fitting the data to eq 2. As can be seen in Figure 7A, there was less DC6C binding to the $\alpha\gamma$ site, inhibited by low D-tubocurarine concentrations, than to the $\alpha\delta$ site, inhibited by higher concentrations, indicating that the $\alpha\gamma$ site has a lower affinity than the $\alpha\delta$ site. This site preference was more pronounced at lower DC6C concentrations (Figure 7A,B). The amount of binding at each site was determined at several DC6C concentrations and the binding ratio plotted against the DC6C concentration (Figure 7B). The limiting ratio at low DC6C concentrations shows that the affinity for the $\alpha\delta$ site is 3−4-fold higher than at the $\alpha\delta$ site. These data were fitted to eq 3 to determine the K_D at each site. The K_D value of 2.9 nM determined for the $\alpha\delta$ site agrees well with the value calculated from the kinetic

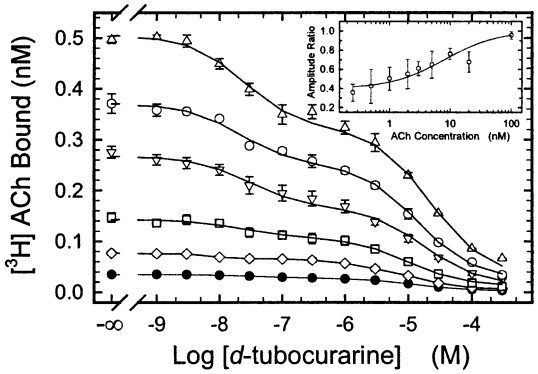

FIGURE 8: ACh binds with higher affinity to the $\alpha\delta$ site than the $\alpha\gamma$ site of the desensitized AChR. AChR-rich membranes (2 nM) were incubated in HTPS, 25 μM proadifen, and the indicated concentrations of D-tubocurarine with the following concentrations of [^{3}H]ACh: 0.25 (●), 0.5 (◇), 1 (□), 2 (▽), 3 (○), and 5 nM (△). [^{3}H]ACh binding was assessed as described in Experimental Procedures as well as for samples containing 1 mM carbamylcholine or no ligand (data not shown). The error bars represent the standard deviations of triplicate determinations. The data were fitted to the two-site inhibition equation (eq 2, —) to determine the binding contribution from each site, $a_{\alpha\gamma}$ and $a_{\alpha\delta}$. In the inset, amplitude ratios, $a_{\alpha\gamma}/a_{\alpha\delta}$, were combined from experiments with ACh concentrations varying up to 100 nM. The plot shows average ratios at each concentration with error bars indicating the standard deviation of 2−10 independent ratio determinations. The solid curve (—) is the best fit to eq 3 with a fixed A of 1. The K values from the fit are as follows: $K_{D\alpha\delta} = 3.2$ nM and $K_{D\alpha\gamma} = 8.0$ nM.

constants (Table 3). The K_D value of 9.4 nM for the $\alpha\gamma$ site remains lower than that predicted from the kinetic constants, but now differs by only 2-fold. Similar results were obtained using epibatidine instead of D-tubocurarine as the site-selective competitor.

To illustrate that the K_D values determined by the ratio of kinetic constants or by the amplitude ratio method are consistent with binding isotherm data, we modeled the binding expected from these values under the conditions shown in Figure 2B (10 nM AChR desensitized by the presence of proadifen). Because this receptor concentration was near the K_D values and within the range of DC6C concentrations used, it was necessary to derive a formula to account for binding as a function of the total ligand concentration added. As shown by the dashed (from k_-/k_+ values, Table 3) and dotted curves (from the amplitude ratio measurements, Table 3) in Figure 2B, the computed binding curves match the data and approximate the best single-site binding curve fit (solid curve).

To determine whether the difference in affinity at the two sites in the desensitized state applied to ACh as well as to DC6C, we carried out similar experiments with [^{3}H]ACh instead of DC6C. As can been seen in the main panel and inset of Figure 8, similar results were achieved, showing that the affinity of ACh also differs among the two sites in the desensitized state with K_Ds of 8 and 3.2 nM for the $\alpha\gamma$ and $\alpha\delta$ sites, respectively. Because of difficulty in determining the ratios with sufficient precision, the absolute K_D values are not likely to be accurate, but the K_D ratio clearly approaches a value of 0.3−0.4 at low [^{3}H]ACh concentrations, a value that is similar to that observed for DC6C. This result shows that this affinity difference is seated in the ACh moiety itself, rather than the fluorophore attached to create DC6C.

DISCUSSION

The data demonstrate three new site-selective characteristics of DC6C binding to desensitized agonist sites of the AChR: distinct DC6C fluorescence emission intensity, distinct dissociation rates, and distinct affinities. In addition, we have shown that D-tubocurarine binding to the $\alpha\gamma$ site can effectively desensitize the $\alpha\delta$ site and determined the binding affinities for epibatidine. The characteristic dissociation rates are particularly important in providing fresh insight into the conformational mechanism of the AChR. As shown in Figure 6C, we can use sequential mixing stopped-flow techniques to measure the extent of DC6C binding to desensitized $\alpha\gamma$ sites and to desensitized $\alpha\delta$ sites as a function of time after mixing with DC6C. In that experiment, the AChR was fully desensitized before mixing by virtue of adding a noncompetitive antagonist. In the case where the AChR is not initially desensitized, we expect to be able to follow the time evolution of DC6C-induced desensitization for each site independently. Such experiments will address whether desensitization is concerted for the two sites and whether intermediate states exist as indicated by the rates of desensitization.

Relative DC6C Fluorescence Intensity at the Agonist Sites. The relatively greater fluorescent emission from DC6C when bound to the $\alpha\delta$ site was unexpected since the results of Martinez et al. (*27*) showed that the DC6C bound at the $\alpha\delta$ site had a shorter average fluorescent lifetime (8 ns) than DC6C bound to the $\alpha\gamma$ site (12 ns). In general, the fluorescent lifetime is proportional to the quantum yield (*25*), and the data of Martinez et al. would predict ~50% greater fluorescence from the $\alpha\gamma$ site. We observe the reverse, a 50% greater fluorescence from the $\alpha\delta$ site. We initially suspected that the discrepancy was due to different degrees of energy transfer at the sites, under our excitation conditions, whereas Martinez et al. had used direct excitation of DC6C at 330 nm. However, titration experiments showed that direct excitation of DC6C at 335 nm yielded even higher relative fluorescence emission from the $\alpha\delta$ site (Table 1 and Figure 1D). The discrepancy between their data and ours is unresolved. Our experiments do indicate that the primary difference in yield must be due to the binding site environment. The dansyl moiety is particularly sensitive to hydrophobicity (*25*), and the difference may reflect the intrinsic differences in amino acids that surround the site, differences in the position of the fluorophore, the presence of a quenching moiety, such as occurs for NBD-acylcholine, another fluorescent ACh derivative (*30*), or differences in the conformational stability of the binding site.

Dissociation Kinetics of DC6C. Our data show distinct rates of dissociation of DC6C from the two agonist binding sites. Because DC6C is an agonist that binds cooperatively to the two sites and desensitizes the AChR, the rates likely reflect dissociation from the high-affinity, desensitized conformation. We examined whether conditions that promote desensitization would affect the rates. Neither low ionic strength nor the presence of desensitizing, noncompetitive antagonists such as proadifen, meproadifen, and phencyclidine substantially affected the rates. This argued that the rates likely reflected the native, microscopic dissociation rates. However, one test of this supposition was whether the rates matched the expected equilibrium constants for binding the

desensitized conformation. The rates of association with desensitized sites were the same for the two sites. Using this rate and the distinct dissociation rates, the calculated equilibrium constant for the $\alpha\delta$ site matched that measured by inhibition of DC6C binding by D-tubocurarine (Figure 7). However, the calculated value for the $\alpha\gamma$ site was modestly (2-fold) higher than the observed equilibrium constant.

The discrepancy between the calculated and measured affinities was apparently larger in the low- and high-ionic strength buffers that we also tested. These buffers contain neither the divalent cations nor the potassium that is present in HTPS. We did not measure the affinities at each site explicitly in these buffers; however, the difference between the calculated values and the equilibrium constant determined by a binding isotherm in the presence of proadifen is 10−20-fold for the $\alpha\gamma$ site (Table 3). Such a large difference should have been apparent in the isotherm. Under these conditions, the observed rate of dissociation from the $\alpha\gamma$ site may reflect more steps than just the microscopic dissociation from the desensitized state. One possibility is that local conformational changes can affect the dissociation rate. Such mechanisms may also account for the $\alpha\gamma$ site dissociation rate being more variable than the $\alpha\delta$ rate observed in HTPS (Table 2).

Agonist dissociation has been examined for another fluorescent ACh analogue, NBD-5-acylcholine. Analysis of dissociation kinetics from the *Electricus electrophorus* AChR yielded rates similar to ours (*31*). Subsequent work on this ligand, using a more complete analysis for the *Torpedo marmorata* AChR, however, gave slower rates of 0.2 and 0.06 s^{-1} (*30*). [^{3}H]ACh dissociation had a rate of 0.2 s^{-1} (*13*), a value that closely matches our observed value for dissociation of DC6C from the $\alpha\delta$ site. Raines and Krishnan (*21*) used DC6C dissociation kinetics as a measure of the amount of net desensitization of the *Torpedo nobiliana* AChR in sequential mixing experiments, although no dissociation rates were reported. Their approach effectively determined the course of desensitization during ligand association. We can now extend this technique to assess desensitization independently at each site using the distinct dissociation rates to differentiate the sites. That this method works is shown in Figure 6C for binding of an agonist to the pre-desensitized AChR.

Dunn and Raftery (*32*) measured dilution-induced dissociation rates for [^{3}H]ACh that were approximately 10-fold slower (0.02 s^{-1}) than those we observed for DC6C. This rate could be increased substantially by inclusion of competing agonist to values similar to those we observe from the $\alpha\delta$ site (~0.1 s^{-1}). They proposed that competing ligands induce faster dissociation by weak binding to a nearby subsite; potentially, this site is the same subsite that can be occupied by larger, bifunctional ligands such as succinyldicholine. Because DC6C is likely to act as such a bifunctional ligand, such an effect ought not affect our measurements. However, it is possible that the discrepancy between dissociation rates determined by dilution versus those determined by competition may have been influenced by a component of rapid rebinding to nearby unoccupied receptors (*33*). For receptors at a high planar density, such as in AChR-rich vesicles, this effect can be substantial (*34*). For DC6C, we also observed substantially slower dissociation when it was induced by dilution without a competing ligand present (X.-Z. Song and S. E. Pedersen, unpublished observations). Whether this effect is due to rapid rebinding can be tested by comparison of dissociation rates from AChR-rich vesicles and a detergent-solubilized AChR.

Desensitized State Binding Affinities. The differences between the two AChR binding sites have been well established for the binding of antagonists such as conotoxins and D-tubocurarine, for the agonist epibatidine, and, to a lesser extent, for carbamylcholine. Epibatidine clearly has a higher affinity for the $\alpha\gamma$ site in the desensitized conformation (Figure 1A; see also ref *11*). Carbamylcholine appears to have a higher affinity for the $\alpha\delta$ site of mouse AChR in the resting state, but apparent affinities in the desensitized state differed by only ~3-fold (*14*). Those values are similar to those observed here for DC6C and [^{3}H]ACh. The difference in agonist affinity for the desensitized state further reaffirms that the site differences extend to this conformation, even for small ligands such as ACh, but to a substantially lesser extent than the resting state affinities, which differ by as much as 100-fold (*2*). In addition, the similar affinity difference between the sites for DC6C and ACh suggests that DC6C is a valid model for the physiological ligand, ACh, where the fluorophore has a minimal influence on the desensitized state affinity. The modest, 3-fold difference in the desensitized state affinity is consistent with the high degree of conservation of amino acids found in the binding pocket of the acetylcholine binding protein. Residues considered important for site-selective binding lie at the periphery of the site, and the influence of many of these residues may be conformational rather than by direct interaction with the ligand. While it is not known whether the acetylcholine binding protein structure represents the desensitized or resting state of the binding site, it appears to approximate the desensitized state (*35*).

Summary and Conclusions. The fluorescence of DC6C differs at the $\alpha\gamma$ and $\alpha\delta$ binding sites, as shown by titration with competitive inhibitors and by the amplitudes of the dissociation kinetics. The DC6C dissociation rates from the two sites differ substantially by 5−10-fold, and the equilibrium dissociation constants for the desensitized state also differ by 3-fold. The $\alpha\delta$ site had higher fluorescence, slower dissociation, and higher affinity than the $\alpha\gamma$ site; however, it is not obvious whether the difference in fluorescence is related to the differences in off-rates and affinity. Nonetheless, in each case, the observations further differentiate the nicotinic AChR sites and provide a quantitative description of DC6C binding kinetics. The characteristic dissociation rates permit us to measure the extent of desensitization independently at each site and establish a basis for experimentally distinguishing concerted models from nonconcerted models of desensitization.

ACKNOWLEDGMENT

We thank Nasrin Latif Shooshtari for excellent technical assistance in carrying out acetylcholine binding assays.

REFERENCES

1. Pedersen, S. E., and Cohen, J. B. (1990) D-Tubocurarine binding sites are located at α-γ and α-δ subunit interfaces of the nicotinic acetylcholine receptor, *Proc. Natl. Acad. Sci. U.S.A. 87*, 2785−2789.

2. Sine, S. M., Claudio, T., and Sigworth, F. J. (1990) Activation of *Torpedo* acetylcholine receptors expressed in mouse fibroblasts. Single channel current kinetics reveal distinct agonist binding affinities, *J. Gen. Physiol. 96*, 395−437.
3. Boyd, N. D., and Cohen, J. B. (1984) Desensitization of membrane-bound *Torpedo* acetylcholine receptor by amine noncompetitive antagonists and aliphatic alcohols: studies of [^{3}H]acetylcholine binding and $^{22}Na^+$ ion fluxes, *Biochemistry 23*, 4023−4033.
4. Sine, S. M., Kreienkamp, H. J., Bren, N., Maeda, R., and Taylor, P. (1995) Molecular dissection of subunit interfaces in the acetylcholine receptor: identification of determinants of α-conotoxin M1 selectivity, *Neuron 15*, 205−211.
5. Papineni, R. V., Sanchez, J. U., Baksi, K., Willcockson, I. U., and Pedersen, S. E. (2001) Site-specific charge interactions of α-conotoxin MI with the nicotinic acetylcholine receptor, *J. Biol. Chem. 276*, 23589−23598.
6. Prince, R. J., and Sine, S. M. (1999) Acetylcholine and epibatidine binding to muscle acetylcholine receptors distinguish between concerted and uncoupled models, *J. Biol. Chem. 274*, 19623−19629.
7. Neubig, R. R., and Cohen, J. B. (1979) Equilibrium binding of [^{3}H]tubocurarine and [^{3}H]acetylcholine by *Torpedo* postsynaptic membranes: stoichiometry and ligand interactions, *Biochemistry 18*, 5464−5475.
8. Krodel, E. K., Beckman, R. A., and Cohen, J. B. (1979) Identification of a local anesthetic binding site in nicotinic postsynaptic membranes isolated from *Torpedo marmorata* electric tissue, *Mol. Pharmacol. 15*, 294−312.
9. Pedersen, S. E., and Papineni, R. V. (1995) Interaction of D-tubocurarine analogs with the *Torpedo* nicotinic acetylcholine receptor. Methylation and stereoisomerization affect site-selective competitive binding and binding to the noncompetitive site, *J. Biol. Chem. 270*, 31141−31150.
10. Xie, Y., and Cohen, J. B. (2001) Contributions of *Torpedo* Nicotinic Acetylcholine Receptor γ-Trp-55 and δ-Trp-57 to Agonist and Competitive Antagonist Function, *J. Biol. Chem. 276*, 2417−2426.
11. Prince, R. J., and Sine, S. M. (1998) Epibatidine Binds With Unique Site and State Selectivity to Muscle Nicotinic Acetylcholine Receptors, *J. Biol. Chem. 273*, 7843−7849.
12. Edelstein, S. J., Schaad, O., Henry, E., Bertrand, D., and Changeux, J. P. (1996) A kinetic mechanism for nicotinic acetylcholine receptors based on multiple allosteric transitions, *Biol. Cybernetics 75*, 361−379.
13. Boyd, N. D., and Cohen, J. B. (1980) Kinetics of binding of [^{3}H]-acetylcholine and [^{3}H]carbamoylcholine to *Torpedo* postsynaptic membranes: slow conformational transitions of the cholinergic receptor, *Biochemistry 19*, 5344−5353.
14. Sine, S. M., and Claudio, T. (1991) γ- and δ-subunits regulate the affinity and the cooperativity of ligand binding to the acetylcholine receptor, *J. Biol. Chem. 266*, 19369−19377.
15. Koshland, D. E., Jr., Nemethy, G., and Filmer, D. (1966) Comparison of experimental binding data and theoretical models in proteins containing subunits, *Biochemistry 5*, 365−385.
16. Neubig, R. R., Boyd, N. D., and Cohen, J. B. (1982) Conformations of *Torpedo* acetylcholine receptor associated with ion transport and desensitization, *Biochemistry 21*, 3460−3467.
17. Elenes, S., and Auerbach, A. (2002) Desensitization of diliganded mouse muscle nicotinic acetylcholine receptor channels, *J. Physiol. 541*, 367−383.
18. Heidmann, T., and Changeux, J. P. (1979) Fast kinetic studies on the interaction of a fluorescent agonist with the membrane-bound acetylcholine receptor from *Torpedo marmorata*, *Eur. J. Biochem. 94*, 255−279.
19. Heidmann, T., and Changeux, J. P. (1979) Fast kinetic studies on the allosteric interactions between acetylcholine receptor and local anesthetic binding sites, *Eur. J. Biochem. 94*, 281−296.
20. Heidmann, T., and Changeux, J. P. (1980) Interaction of a fluorescent agonist with the membrane-bound acetylcholine receptor from *Torpedo marmorata* in the millisecond time range: resolution of an "intermediate" conformational transition and evidence for positive cooperative effects, *Biochem. Biophys. Res. Commun. 97*, 889−896.
21. Raines, D. E., and Krishnan, N. S. (1998) Transient low-affinity agonist binding to *Torpedo* postsynaptic membranes resolved by using sequential mixing stopped-flow fluorescence spectroscopy, *Biochemistry 37*, 956−964.
22. Pedersen, S. E., Dreyer, E. B., and Cohen, J. B. (1986) Location of ligand-binding sites on the nicotinic acetylcholine receptor α-subunit, *J. Biol. Chem. 261*, 13735−13743.
23. Waksman, G., Fournie-Zaluski, M. C., and Roques, B. (1976) Synthesis of fluorescent acyl-cholines with agonistic properties: pharmacological activity on *Electrophorus electroplaque* and interaction in vitro with *Torpedo* receptor-rich membrane fragments, *FEBS Lett. 67*, 335−342.
24. Song, X. Z., and Pedersen, S. E. (2000) Electrostatic interactions regulate desensitization of the nicotinic acetylcholine receptor, *Biophys. J. 78*, 1324−1334.
25. Lakowicz, J. R. (1983) *Principles of Fluorescence Spectroscopy*, Plenum, New York.
26. Cheng, Y., and Prusoff, W. H. (1973) Relationship between inhibition constant (K_i) and the concentration of inhibitor which causes 50% inhibition of an enzymatic reaction, *Biochem. Pharmacol. 22*, 3099−3108.
27. Martinez, K. L., Corringer, P. J., Edelstein, S. J., Changeux, J. P., and Merola, F. (2000) Structural differences in the two agonist binding sites of the *Torpedo* nicotinic acetylcholine receptor revealed by time-resolved fluorescence spectroscopy, *Biochemistry 39*, 6979−6990.
28. Sine, S., and Taylor, P. (1979) Functional consequences of agonist-mediated state transitions in the cholinergic receptor. Studies in cultured muscle cells, *J. Biol. Chem. 254*, 3315−3325.
29. Heidmann, T., Bernhardt, J., Neumann, E., and Changeux, J. P. (1983) Rapid kinetics of agonist binding and permeability response analyzed in parallel on acetylcholine receptor rich membranes from *Torpedo marmorata*, *Biochemistry 22*, 5452−5459.
30. Prinz, H., and Maelicke, A. (1992) Ligand binding to the membrane-bound acetylcholine receptor from *Torpedo marmorata*: a complete mathematical analysis, *Biochemistry 31*, 6728−6738.
31. Prinz, H., and Maelicke, A. (1983) Interaction of cholinergic ligands with the purified acetylcholine receptor protein. II. Kinetic studies, *J. Biol. Chem. 258*, 10273−10282.
32. Dunn, S. M., and Raftery, M. A. (1997) Agonist binding to the *Torpedo* acetylcholine receptor. 1. Complexities revealed by dissociation kinetics, *Biochemistry 36*, 3846−3853.
33. Lagerholm, B. C., and Thompson, N. L. (1998) Theory for ligand rebinding at cell membrane surfaces, *Biophys. J. 74*, 1215−1228.
34. Lagerholm, B. C., Starr, T. E., Volovyk, Z. N., and Thompson, N. L. (2000) Rebinding of IgE Fabs at haptenated planar membranes: measurement by total internal reflection with fluorescence photobleaching recovery, *Biochemistry 39*, 2042−2051.
35. Unwin, N., Miyazawa, A., Li, J., and Fujiyoshi, Y. (2002) Activation of the nicotinic acetylcholine receptor involves a switch in conformation of the α subunits, *J. Mol. Biol. 319*, 1165−1176.

BI027405B